Analyst

PAPER

Check for updates

Direct low field J-edited diffusional proton NMR spectroscopic measurement of COVID-19 inflammatory biomarkers in human serum†

Philipp Nitschke,*[a] Samantha Lodge, [iD] [a] Drew Hall,[a] Hartmut Schaefer,[b] Manfred Spraul,[b] Nieves Embade,[c] Oscar Millet,[c] Elaine Holmes,[a,d] Julien Wist [iD] *[a,e] and Jeremy K. Nicholson*[a,f]

A JEDI NMR pulse experiment incorporating relaxational, diffusional and J-modulation peak editing has been implemented for a low field (80 MHz proton resonance frequency) spectrometer system to measure quantitatively two recently discovered plasma markers of SARS-CoV-2 infection and general inflammation. JEDI spectra capture a unique signature of two biomarker signals from acetylated glycoproteins (Glyc) and the supramolecular phospholipid composite (SPC) signals that are relatively enhanced by the combination of relaxation, diffusion and J-editing properties of the JEDI experiment that strongly attenuate contributions from the other molecular species in plasma. The SPC/Glyc ratio data were essentially identical in the 600 MHz and 80 MHz spectra obtained ($R^2 = 0.97$) and showed significantly different ratios for control ($n = 28$) *versus* SARS-CoV-2 positive patients ($n = 29$) ($p = 5.2 \times 10^{-8}$ and 3.7×10^{-8} respectively). Simplification of the sample preparation allows for data acquisition in a similar time frame to high field machines (~4 min) and a high-throughput version with 1 min experiment time could be feasible. These data show that these newly discovered inflammatory biomarkers can be measured effectively on low field NMR instruments that do not not require housing in a complex laboratory environment, thus lowering the barrier to clinical translation of this diagnostic technology.

[a]*Australian National Phenome Centre and Computational and Systems Medicine, Health Futures Institute, Murdoch University, Harry Perkins Building, Perth, WA6150, Australia. E-mail: Philipp.Nitschke@murdoch.edu.au, Julien.Wist@murdoch.edu.au, Jeremy.Nicholson@murdoch.edu.au*

[b]*Bruker Biospin GmbH, Rudolf-Plank Strasse 23, 76275 Ettlingen, Germany*

[c]*Precision Medicine and Metabolism Laboratory, CIC bioGUNE, Parque Tecnológico de Bizkaia, Bld. 800, 48160 Derio, Spain*

[d]*Department of Metabolism, Digestion and Reproduction, Faculty of Medicine, Imperial College London, Sir Alexander Fleming Building, South Kensington, London SW7 2AZ, UK*

[e]*Chemistry Department, Universidad del Valle, Cali 76001, Colombia*

[f]*Institute of Global Health Innovation, Faculty of Medicine, Imperial College London, Level 1, Faculty Building, South Kensington Campus, London, SW7 2NA, UK*

†Electronic supplementary information (ESI) available: Fig. S1: Comparison of solvent suppressed proton spectra and JEDI for a healthy control at 600 and 80 MHz. Fig. S2: Aliphatic 600 MHz ^{1}H NMR region of serum at 310 and 298 K. Fig. S3: 600 MHz JEDI spectra of SPC and Glyc at 310 and 298 K. Fig. S4: Sequence of Pulsed Gradient Spin Echo (PGSE). Fig. S5: Sequence of Pulsed Gradient Perfect Echo (PGPE). Fig. S6: JEDI-PGSE and JEDI-PGPE of serum at 80 MHz. Fig. S7: Comparison of the Glyc region in a serum sample at 80 MHz and 600 MHz by JEDI. Fig. S8: Statistical analyses comparing SPC/Glyc JEDI-PGPE measurements at 600 MHz 310 K (IVDr) and 600 MHz 298 K with SPC/Glyc measurements at 80 MHz 298 K. Fig. S9: Chemical shift sensitivity of SPC and Glyc in a serum sample at 80 MHz. Fig. S10: Effects of varying plasma concentration and number of scans/experimental time on JEDI-PGPE at 80 MHz. See DOI: https://doi.org/10.1039/d2an01097f

Introduction

High field proton Nuclear Magnetic Resonance (NMR) spectroscopy of biofluids has been applied to numerous metabolic diseases and toxic states for over three decades in order to interrogate mechanistic processes and also as a diagnostic platform.[1] However, there is a significant challenge in translating clinical biomarker discovery platforms and new clinical biomarker measurements into practical field-deployable solutions that could work in the clinic or routine laboratory. High field NMR has a high capital cost and is mainly only available in top-end discovery laboratories or hospitals. In general, the history of metabolic profiling using high resolution biofluid NMR, has mainly followed an expected trajectory of using ever increasing magnetic fields, which benefit from improved dispersion and sensitivity.[2–4] Despite the tremendous success of benchtop NMR systems in other fields like online reaction monitoring,[5–8] offline reaction study,[9] teaching,[10,11] forensic applications,[12,13] and quality control,[14–16] there have been few successful deployments of low field NMR spectrometers for clinical detection of disease because of biochemical and spectral complexity.[6,17–19] Thus, although low field NMR has potential as a disease diagnostic exploratory platform, its limited

use for biofluids can be explained by the implicit higher signal overlap, which confounds detection or quantification of signals with corresponding degradation of signal/diagnostic fidelity. In addition, benchtop NMR magnets are extremely sensitive to temperature fluctuations and it is challenging to reach the same level of spectral stability as displayed by high-field superconducting magnet systems. Recent advances in permanent magnet technology have enabled the production of low footprint benchtop NMR systems that can use the same sophisticated spin physics experiments as research machines and so can provide opportunities for more routine clinical deployment. Notwithstanding the challenges, there is an increasing demand for new diagnostic markers at or near point-of-care, where benchtop systems are economically more viable, placing a critical need on developing low field or benchtop diagnostics.[17] A key advantage of NMR spectroscopy over other diagnostic platforms is its non-invasive nature which enables the interrogation of molecular and physical interactions and molecular motions in complex mixtures that can carry extra diagnostic information over and above pure concentration data.

COVID-19 has presented major scientific, medical and socioeconomic challenges to the world that require multilevel solutions including new diagnostics and methods to evaluate the disease process[20–23] and recovery from it.[24,25] We previously described the complex *metabolic phenoconversion* process that characterises the multi-organ involvement of the SARS-CoV-2 infection process; *e.g.* SARS-CoV-2-(+) patients could be effectively distinguished from healthy controls modelling untargeted ^{1}H NMR data (Fig. 1A). Phenoconversion from a healthy into an infected state is associated with changes in the concentrations of a wide range of metabolic entities (lipoproteins, glycoproteins, amino acids, lipids and other metabolites) that can be derived from NMR spectroscopic and mass spectrometric data,[26–28] and which result in distinctive embedded biomarker features including some of those previously observed in diabetes,[29,30] cardiovascular disease,[31–35] liver dysfunction,[36,37] neurological disruption[38] and inflammation.[39,40] Many of these pathological changes can be observed using a variety of NMR experiments on blood plasma and these changes are robust to sample handling with standardised protocols[41,42] and were also observed by others.[22,43–45]

Well resolved *N*-acetyl signals from glycosylated amino sugar residues from side-chains of acute phase reactive proteins such as α-1 *N*-acetyl-glycoprotein in NMR spectra of blood plasma were first reported by Bell *et al.*,[46] and are elevated in multiple inflammatory states, such as obesity,[47] diabetes,[48] cardiovascular disease,[49,50] rheumatoid arthritis,[51] systemic immune-pathological conditions such as HIV infection,[52] systemic lupus erythematosus[53] and COVID-19.[26,54] These signals are now referred to as GlycA and GlycB[21] or just Glyc as the sum of the GlycA and GlycB. GlycA (δ 2.03 ppm) and GlycB (δ 2.07 ppm) are highly correlated and are postulated to be composites of *N*-acetyl signals from five main proteins: α-1-acid glycoprotein, α-1-antichymotrypsin, α-1-antitrypsin, haptoglobin and transferrin.[53] We recently reported that

Glyc signals are significantly elevated in COVID-19 patients and are strongly associated with infection positivity.[26,27] In addition to Glyc, the supramolecular phospholipid composite (SPC) stemming from trimethylammonium residues in lipoprotein bound phospholipids was recently discovered as another inflammatory marker defining SARS-CoV-2 infection and SPC can also be used as a surrogate to gauge cardiovascular disease risk by analysis of its respective composite sub-regions.[21,54] SPC was first quantified by DIffusion and Relaxation Editing (DIRE) NMR spectroscopy, which allows for integration of the peak by combining diffusion editing and T_2-relaxation.[21] Both candidate biomarkers SPC and Glyc were found to be distinguishing features under inflammatory conditions showing a distinct inverse relationship in the case of SARS-CoV-2 infection, with an increase of Glyc and a decrease of SPC (Fig. 1B), which can be expressed as the SPC/Glyc ratio for inflammation assessment.[20]

DIRE NMR spectroscopy was originally proposed as an experiment to enhance signals from molecules exhibiting slow translational diffusion, but with high segmental motional freedom.[55] These requirements are satisfied by plasma glycoproteins and molecules constrained within certain lipoprotein sub-compartments.[56,57] In a recent study we showed that measurement precision and sensitivity for both Glyc and SPC peaks could be improved using an additional J filter.[20] This J-edited diffusion and relaxation (JEDI) NMR technique introduces destructive interference for signals with complex coupling interactions (Fig. 1C and D) thus minimising spectral interference and particularly enhances the quantitative integration accuracy of the Glyc peak(s). In addition, JEDI also yields increased signal to noise over DIRE due to shorter relaxation periods during the sequence. Our previous studies were performed on high field (600 MHz) IVDr NMR instruments that are widely used in clinical biochemistry studies to measure lipoprotein subfractions. Given the spectral simplification that JEDI experiments confer on complex mixtures, it makes them an ideal approach for low field NMR applications as they compensate both for the decreased dispersion and the more pronounced strong coupling effects at lower field. Adapted versions of JEDI experiments could provide comparable diagnostic capabilities, *e.g.* the SPC/Glyc ratio in reasonable NMR scanning times using more accessible low field NMR systems that are less costly and more readily field deployable.

Results and discussion

We demonstrate that the translation of the JEDI method for the detection and quantification of SPC and Glyc (GlycA + GlycB) from high field NMR to benchtop 80 MHz NMR is feasible. Furthermore, it can be executed in similar timeframes as high field measurements. The determination of the SPC/Glyc ratio was performed for both 600 MHz and 80 MHz field strengths at different temperatures for a cohort of SARS-CoV-2-(+) and their controls.

Fig. 1 Schematic showing the timeline and information summary for SPC and Glyc since their definition as candidate inflammatory markers of COVID-19 in 2020 (A and B), their subsequent quantitation in 2021 (C and D) and translation of detection methods for SPC and Glyc from 600 MHz to 80 MHz in 2022 (E and F). (A) OPLS of healthy controls (blue triangles) and SARS-CoV-2-positive patients using 1D ^{1}H NMR input data effectively distinguishes between both groups (B) OPLS loadings show a high contribution and an inverse relationship between SPC and Glyc with SPC decreasing and Glyc increasing during COVID-19 due to acute inflammation. (A) and (B) was published in ref. 54 and is reproduced here under the terms of Creative Commons Attribution 4.0 licence. (C) 1D ^{1}H with solvent suppression at 600 MHz (310 K) demonstrating the high peak convolution for SPC (red) and Glyc (blue) in an unedited experiment. (D) JEDI spectrum at 600 MHz (310 K) using relaxation, diffusion and J-editing to enable direct quantitation of SPC and Glyc by integration (E) 1D ^{1}H NMR with solvent suppression at 80 MHz (298 K) showing the decreased signal dispersion and lower sensitivity compared to 600 MHz (C). At 80 MHz SPC is fully overlapped with Glucose peaks and Glyc fully overlapped with lipid resonances. (F) JEDI spectrum at 80 MHz (298 K) eliminates all overlapping peaks. More importantly, the lower dispersion at the benchtop field is not an issue, due to the extensive spectral editing of JEDI.

Acquisition of the aliphatic region of a 1D ^{1}H NMR spectrum (600 MHz, 310 K) of human serum allows for the detection of SPC (red) and Glyc (blue), but any quantitation of SPC and Glyc is hindered due to extensive convolution with small molecules, lipoproteins and protein background (Fig. 1C and S1A†). SPC and Glyc can be made spectroscopically accessible using JEDI spectroscopy, which combines diffusion, relaxation and J-editing to effectively remove all resonances interfering with SPC and Glyc. Fig. 1D shows the JEDI spectrum of 1C at 600 MHz, which enables direct quantitation of SPC and Glyc by simple integration. Apart from the SPC and Glyc signals, the JEDI spectrum is essentially void of other resonances. JEDI only contains residual lipoprotein peaks at δ 0.88, δ 1.28 and δ 2.77 ppm, the residual –C**H**– sugar residues belonging to the sugar moieties of N-acetylglucosamine (GlcNAc) and N-acetylneuraminic acid (Neu5Ac) of Glyc from δ 3.5–4.1 ppm, the choline moiety methylene groups at δ 3.69 and δ 4.32, and residual protein peaks in the aromatic region in addition to the main peaks SPC and Glyc (Fig. S1B†), whereas a 1D ^{1}H NMR spectrum of serum usually contains over a hundred peaks.[58,59] Considering that the JEDI experiment only refo-

cuses uncoupled protons, i.e. singlets like SPC and Glyc, and given that the heavy pulse editing removes almost all resonances from the spectrum, JEDI presents an ideal candidate pulse sequence for application at lower fields as it intrinsically avoids two of the main issues encountered with benchtop NMR systems: namely, severely decreased spectral dispersion and more pronounced interference of strong coupling.[60,61] This can be confirmed by acquisition of a regular 1D ^{1}H NMR at 80 MHz (Fig. 1E) which also demonstrates the markedly lowered signal to noise (S/N) at lower field. Comparing the 80 MHz spectrum (Fig. 1E) to the 600 MHz equivalent (Fig. 1C) it is evident that the low field spectrum presents an amalgamation of broad features rather than many distinct peaks with a broad lipoprotein + protein background. SPC (red) and Glyc (blue) can still be gauged but are not just partially but indistinguishably overlapped with other resonances rendering attempts for relative quantification impractical. Other features like the main lipoprotein resonances, glucose and various other small molecules can still be detected, but also suffer from heavy convolution and/or low S/N (Fig. S1C†). Recording a spectrum with the JEDI method at 80 MHz gives a much

clearer picture (Fig. 1F). Similar to the JEDI spectrum at 600 MHz (Fig. 1D), the spectrum shows SPC and Glyc to be the dominant features. As both the $-^+NCH_3$ residues of SPC and the *N*-acetyl residues of Glyc stem from uncoupled spin systems, they are unaffected by strong coupling effects at lower fields and are Fourier transformed into singlet peaks. In addition, due to the heavy editing of JEDI based on diffusion, relaxation and J-editing, almost all other resonances are eliminated compensating for the reduced dispersion at 80 MHz. This results in clean peaks for SPC and Glyc, which can be simply integrated for quantitation.

For the successful implementation and translation of the JEDI experiments from 600 to 80 MHz, various practical and theoretical considerations had to be taken into account. Currently the 80 MHz only allows for operation at a fixed temperature of 298 K, whereas serum or plasma measurements according to IVDr procedures are carried out at 310 K.[62] Lower temperatures in serum lead to a change in chemical shifts,[63] different coupling constants and a different lipoprotein profile (shape of the composite peaks), because the lipoprotein signal response depends on the mobility of the varying sub-components, which are further immobilised at reduced temperature.[56] In addition, lower temperatures lead to smaller diffusion coefficients and relaxation times due to increased solvent viscosity,[64] which are critical for JEDI editing. The effect of lower temperature on human serum can be clearly seen when comparing solvent suppressed ^1H NMR spectra at 310 and 298 K (Fig. S2†). The signal responses from all macromolecular components *i.e.* protein background and lipoproteins are significantly reduced at 298 K. This includes the two biomarkers of SPC and Glyc, which stem from superimposed lipoprotein (SPC) and glycoprotein glycan (Glyc) peaks respectively.[20,21] A more detailed picture of the effects of lowered temperature to SPC and Glyc can be taken from the JEDI spectra (Fig. S3†). Here, SPC is significantly reduced by ∼30% in peak intensity at 298 K compared to 310 K (Fig. S3A†). In addition, the different regions of SPC are affected differently. The high frequency part of SPC=(Fig. S3B†), which stems from LDL lipoproteins is almost completely eliminated at 298 K compared to the low frequency part of SPC, stemming from HDL lipoproteins.[31] Similar to SPC, Glyc is also reduced by ∼20% in intensity at lower temperature (Fig. S3C†). Here, the intensity of the Glyc sub-regions, GlycA and GlycB are affected the same and only their frequencies are slightly altered with GlycB shifting to 2.4 Hz higher frequency with respect to GlycA. Notably, the residual lipoprotein peaks ($-CH_2CH=CH-$), which are overlapped with Glyc, are also strongly reduced at lower temperatures further improving the editing capabilities of JEDI (Fig. S3D†). The diffusional strength of JEDI was still found to be sufficient at 298 K and no small molecule resonances were detected.

For the translation to 80 MHz operating at 298 K, two possible JEDI pulse sequences were considered; the JEDI pulsed gradient spin echo (JEDI-PGSE; Fig. S4†) and the pulsed gradient perfect echo (JEDI-PGPE; Fig. S5†) (ESI:† basic pulse sequences). Both were introduced previously, with

the JEDI-PGPE being deemed the go-to sequence at 600 MHz yielding a high S/N ratio combined with good lipoprotein suppression.[20] The JEDI-PGSE yields a higher S/N, which is offset by reduced lipoprotein suppression and some baseline issues, but due to the lower sensitivity of benchtop NMR systems, S/N is one of the most crucial factors. Porting the methods to 80 MHz is straightforward and only requires adjustment of the time domain data points, due to the lower field (see Experimental section). Additionally, the previously proposed z-filter for both JEDI-PGSE and JEDI-PGPE had to be removed as the potency of the purge gradient was not strong enough on the benchtop system to remove a re-introduced water signal during the z-filter. The respective JEDI spectra of healthy control serum acquired with JEDI-PGSE and JEDI-PGPE are shown in Fig. S6.† Both yield clear peaks for SPC and Glyc void of obstructive overlap preventing analysis. The JEDI-PGSE demonstrated a higher S/N over the JEDI-PGPE (factor ∼1.6), which is in line with experiments at 600 MHz.[20] In contrast, the JEDI-PGPE yielded a flatter baseline and omitted an antiphase residue from δ 3.4–3.8 ppm, which might make the JEDI-PGPE more robust to outliers and thus more suitable for high-throughput applications. The second biomarker, Glyc, can be detected as a lone but uneven singlet (Fig. S7†). This is due to the reduced frequency difference of the Glyc subregions GlycA and GlycB, which coalesce into a single peak at 80 MHz. Using a Gaussian apodization and longer experimental time (2k scans), both GlycA and GlycB can still be discerned at 80 MHz (Fig. S7†). In summary, both JEDI pulse sequences produce a spectrum with clear peaks for SPC and Glyc, that allow for straightforward quantification by integration.

The performance of the 80 MHz JEDI experiment at 298 K against its corresponding 600 MHz counterparts at 298 and 310 K were investigated using a cohort of SARS-CoV-2-(+) patients (*n* = 29) and healthy controls (*n* = 28) described elsewhere.[54] The cohort is expected to show highly increased values for Glyc and decreased values for SPC in the COVID patients resulting in a lowered SPC/Glyc ratio compared to the healthy controls.

The JEDI spectra at 600 MHz were acquired with the JEDI-PGPE sequence at the two temperatures of 310 K, which is the standard temperature for IVDr acquisition and 298 K, which is the fixed operating temperature of the benchtop device. The 80 MHz spectra were acquired with the JEDI-PGPE and the JEDI-PGSE sequence. Comparison of the SPC/Glyc ratio at 600 MHz, 310 K and 80 MHz at 298 K (Fig. 2A) shows a clear distinction between healthy controls and SARS-CoV-2-(+) patients for both fields ($p = 5.2 \times 10^{-8}$ and 3.7×10^{-8} respectively) using the JEDI-PGSE experiment on the 80 MHz. A similar result is achieved comparing the distinction for 600 MHz, to 80 MHz both at 298 K ($p = 3.7 \times 10^{-8}$ and 3.7×10^{-8} respectively) (Fig. 2B). A linear fit of the data for 600 MHz, 310 K against 80 MHz indicated high correlation of the SPC/Glyc ratios (R^2 of 0.93) at both fields (Fig. 2C) suggesting that the method can not only provide an overall distinction between COVID-(+) and healthy controls, but also the individ-
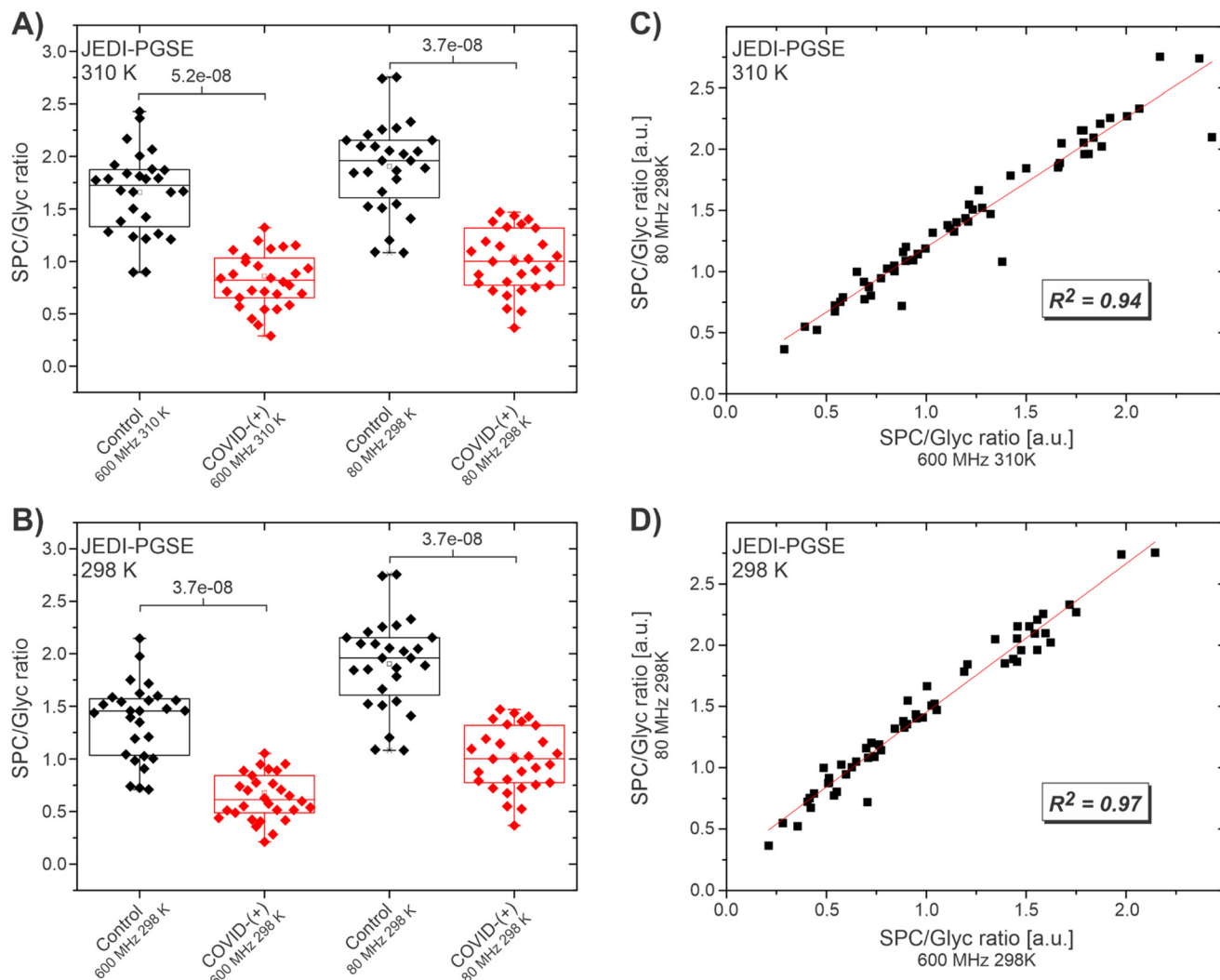
Fig. 2 Statistical analyses comparing SPC/Glyc JEDI measurements at 600 MHz 310 K (IVDr) and 600 MHz 298 K with SPC/Glyc measurements at 80 MHz 298 K. (A) Box plots showing the SPC/Glyc ratio for healthy controls (black) and COVID-(+) samples measured by JEDI-PGSE at 600 MHz 310 K and 80 MHz 298 K; both readily distinguishing between controls and COVID-(+) samples. (B) Box plots showing the SPC/Glyc ratio for healthy controls (black) and COVID-(+) (red) samples at 600 MHz 298 K and 80 MHz 298 K; both readily distinguishing between controls and COVID-(+) samples. (C) Linear fit for the relationship of SPC/Glyc at 600 MHz 310 K and 80 MHz. (D) Linear fit for the relationship of SPC/Glyc at 600 MHz 298 K and 80 MHz.

ual SPC/Glyc ratios per sample can be faithfully reproduced. A higher correlation (R^2 of 0.97) was achieved when comparing the two fields at the same temperature (Fig. 2D). The higher correlation at 298 K is expected due to the slight spectral changes between 310 and 298 K like reduced/eliminated SPC-B contribution in SPC at lower temperatures, which leads to slight offsets when comparing 600 MHz at 310 K to 80 MHz at 298 K. Repeating the same experiments with the JEDI-PGPE experiment revealed a similar picture (Fig. S8†). For both temperatures, 310 and 298 K, a clear distinction was witnessed between SARS-Cov-2-(+) patients and healthy controls (Fig. S8A and B†). In addition, the linear fits of the SPC/Glyc ratios showed the same trend as for the JEDI-PGSE yielding a high correlation ($R^2 = 0.93$) for 600 MHz, 310 K and ($R^2 = 0.97$) for

600 MHz, 298 K against the 80 MHz SPC/Glyc ratios (Fig. S8C and D†). This confirms that the JEDI-PGPE is also a valuable option despite its lower S/N, while providing the option with better baseline stability and residual lipoprotein suppression for outliers. Although the linear fits for the SPC/Glyc ratio for 600 MHz against 80 MHz with JEDI-PGSE and JEDI-PGPE yielded high correlations, T_1 relaxation changes according to the field strength increased with lower field. Moreover, the sequences for the low field application were slightly modified to fit the low field application. This explains the subtle variations in the mean SPC/Glyc ratio between high and lower fields observed in Fig. 2A and B.

After such promising results, we went on to investigate the impact of sample preparation and experimental parameters on

80 MHz spectra. Although, JEDI yields the same results at 600 and 80 MHz, samples prepared according to IVDr procedures (serum/plasma and buffer in a 1 : 1 ratio) lead to ~15 min experimental times at 80 MHz as the lower S/N at low field has to be compensated by a higher number of scans (see section Materials and Methods). In order to reduce the measurement time to make high throughput applications feasible, we excluded the addition of a buffer to double the amount of plasma in the sample. Usually, a buffer is added for NMR serum analysis to ensure a high chemical shift reproducibility for accurate lipoprotein analysis and small molecule quantification; pH control might not be necessary because of the high chemical shift stability of SPC and Glyc. Basic NMR theory tells us that twice the amount of sample leads to a four times reduction of measurement time to achieve the same S/N ratio.[65] This was confirmed by acquiring a JEDI spectrum for the same sample with (Fig. 3A) and without buffer dilution (Fig. 3B). As expected, both spectra yielded similar S/N ratios for SPC and Glyc with the advantage of the undiluted plasma

reducing the possible measurement time for JEDI at 80 MHz to ~4 min, while retaining sufficient signal for analyses. Furthermore, we shortened the measurement times until reaching the theoretical limit of quantification for JEDI experiments at 80 MHz, which is commonly accepted at S/N ≥ 10. Fig. 3C depicts a series of JEDI-PGSE spectra from a healthy control serum sample (*i.e.* SPC high, Glyc low) with increasing number of scans (no dummy scans) leading to a congruent experimental time. SPC as the more intensive peak reaches a SN ≥ 10 with as little as 2 scans or a measurement time of 7 s. A sufficient S/N for Glyc is achieved after 16 scans or 57 s resulting in a S/N of 28.71 for SPC under these conditions (Fig. 3C, green projection). Thus, 16 scans could suffice for the diagnostic test as Glyc usually increases and SPC (S/N of ~30) is not expected to decrease by more than ~30–40%, under inflammatory conditions. This suggests that an experiment time of under 1 minute might be feasible for adequate measurement of the SPC/Glyc ratio to determine inflammation in human serum. In addition, it should be noted that, as the
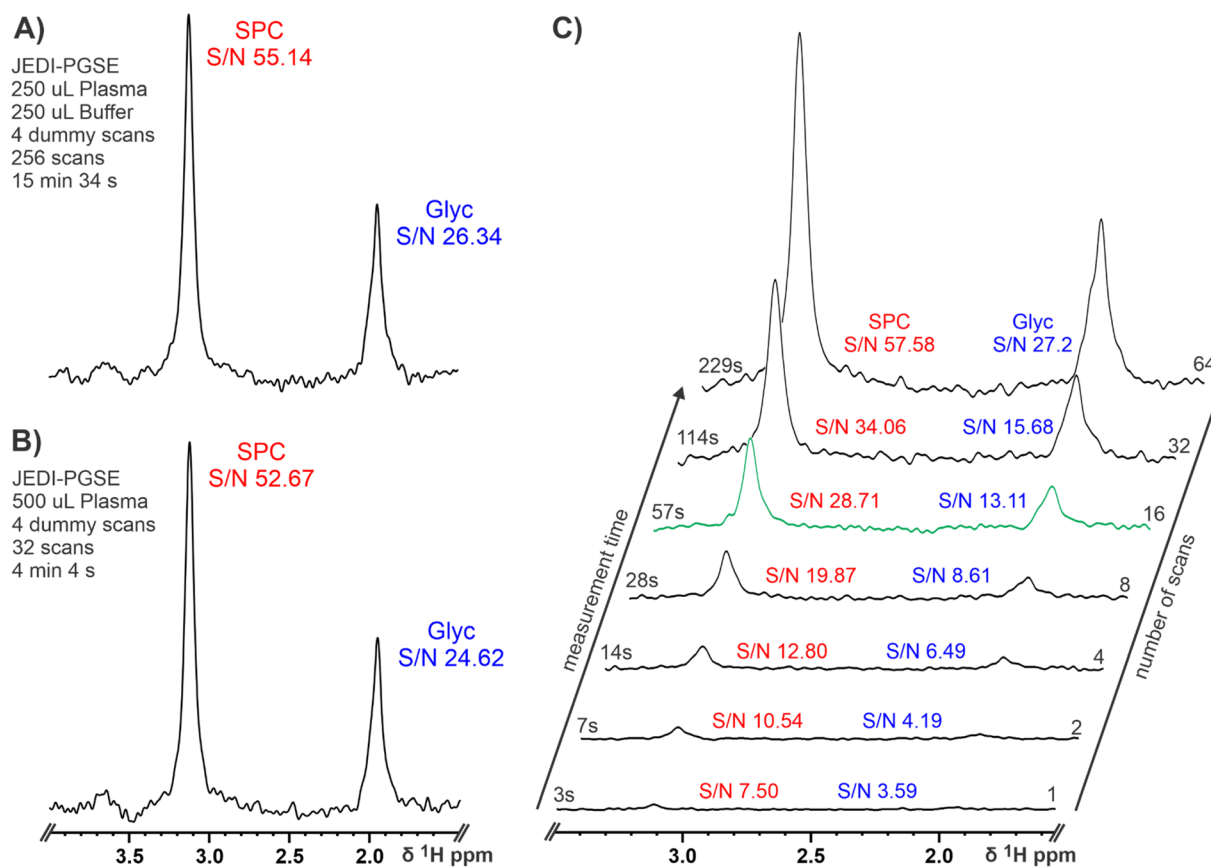
Fig. 3 Effects of varying plasma concentration and number of scans/experimental time on JEDI at 80 MHz. (A) Excerpt of a healthy control JEDI-PGSE spectrum at 80 MHz focusing on SPC and Glyc. The sample was prepared according to IVDr procedures, diluting the plasma 1 : 1 with a buffer (see Material and methods) and the resulting required experimental parameters are shown. (B) Excerpt of the same healthy control JEDI-PGSE spectrum as in A at 80 MHz focusing on SPC and Glyc. The sample was prepared without buffer dilution (see Materials and Methods) resulting in a four times reduction in measurement time, while retaining a similar S/N for SPC and Glyc. (C) Excerpts of healthy control JEDI-PGSE spectra at 80 MHz with increasing number of scans (no dummy scans)/increasing experimental time. Considering a S/N ≥ 10 as limit of detection, it can be presumed that an experimental time of ~1 min could be sufficient for the acquisition of JEDI-PGSE spectra at 80 MHz for the quantitation of SPC and Glyc.

80 MHz system does not require individual sample shimming and due to the chemical shift stability of SPC and Glyc, the required experimental times will not be increased by additional "sample preparation" in the magnet and also extensive sample temperature equilibration might be unnecessary (see Fig. S9†). Hence, including the time for 90° pulse calibration (~10 s) and sample exchange by robotics (~75 s for combined injection and ejection) a real time sample throughput of ~1 sample per 2.5 min could be envisioned. Repeating the procedure of increasing number of scans with the JEDI-PGPE experiment showed the expected result of a lower S/N experiment (Fig. S10†). Instead of reaching sufficient S/N ≥ 10 for SPC and Glyc after 16 scans in under one minute, the JEDI-PGPE requires 32 scans or two minutes for comparable results.

Conclusion

We demonstrated that the detection and quantification of the inflammatory markers SPC and Glyc and the resulting SPC/Glyc ratio with an 80 MHz NMR spectrometer is both possible and applicable. Using JEDI, the main drawbacks of a low field spectrometer *i.e.*, reduced dispersion and strong coupling effects, are successfully circumvented using the underlying triple-editing of diffusion, relaxation and J-editing. Investigation of a SARS-CoV-2-(+) cohort showed that the SPC/Glyc ratio can be successfully reproduced from 600 MHz at the commonly used 310 K as well as 298 K matching the 80 MHz temperature by simple integration of the biomarkers. In addition, omitting sample dilution buffer could successfully decrease the experimental time to under five minutes making high throughput applications accessible. Further experiments with varying number of scans and experimental times suggested the potential of a <1 minute experiment for the quantification of the SPC/Glyc ratio. Overall, JEDI experiments at a low magnetic field strength of 80 MHz for the determination of the SPC/Glyc ratio showed that benchtop applications of serum and plasma can be feasible and time efficient for biomarker investigations and high-throughput analyses. We believe these findings will open the pathway to focus on further investigations of human serum, plasma and other biofluids at low magnetic fields.

Author contributions

JKN, EH, JW, PN, HS, MS and OM conceptualised the project. PN and DH performed all experiments. PN, SL and JW curated and analysed the data. NE and OM provided the samples. All authors wrote and reviewed the manuscript.

Conflicts of interest

There are no conflicts to declare.

Acknowledgements

References

1 I. Garcia-Perez, J. M. Posma, J. I. Serrano-Contreras, C. L. Boulangé, Q. Chan, G. Frost, J. Stamler, P. Elliott, J. C. Lindon, E. Holmes and J. K. Nicholson, *Nat. Protoc.*, 2020, **15**, 2538–2567.

2 J. K. Nicholson, M. J. Buckingham and P. J. Sadler, *Biochem. J.*, 1983, **211**, 605–615.

3 I. D. Nicholson and J. K. Wilson, *Prog. Nucl. Magn. Reson. Spectrosc.*, 1989, **21**, 449–501.

4 J. K. Nicholson, P. J. Foxall, M. Spraul, R. D. Farrant and J. C. Lindon, *Anal. Chem.*, 1995, **67**, 793–811.

5 N. Zientek, C. Laurain, K. Meyer, A. Paul, D. Engel, G. Guthausen, M. Kraume and M. Maiwald, *Magn. Reson. Chem.*, 2016, **54**, 513–520.

6 J. Giberson, J. Scicluna, N. Legge and J. Longstaffe, in *Annual Reports on NMR Spectroscopy*, ed. G. A. Webb, Academic Press, 2021, vol. 102, pp. 153–246.

7 D. Cortés-Borda, E. Wimmer, B. Gouilleux, E. Barré, N. Oger, L. Goulamaly, L. Peault, B. Charrier, C. Truchet, P. Giraudeau, M. Rodriguez-Zubiri, E. Le Grognec and F.-X. Felpin, *J. Org. Chem.*, 2018, **83**, 14286–14299.

8 R. Legner, A. Wirtz, T. Koza, T. Tetzlaff, A. Nickisch-Hartfiel and M. Jaeger, *Biotechnol. Bioeng.*, 2019, **116**, 2874–2883.

9 M. V. Silva Elipe and R. R. Milburn, *Magn. Reson. Chem.*, 2016, **54**, 437–443.

10 S. D. Riegel and G. M. Leskowitz, *Trends Anal. Chem.*, 2016, **83**, 27–38.

11 I. J. Lawson, C. Ewart, A. Kraft and D. Ellis, *Magn. Reson. Chem.*, 2020, **58**, 1256–1260.

12 J. Duffy, A. Urbas, M. Niemitz, K. Lippa and I. Marginean, *Anal. Chim. Acta*, 2019, **1049**, 161–169.

13 L. H. Antonides, R. M. Brignall, A. Costello, J. Ellison, S. E. Firth, N. Gilbert, B. J. Groom, S. J. Hudson, M. C. Hulme, J. Marron, Z. A. Pullen, T. B. R. Robertson, C. J. Schofield, D. C. Williamson, E. K. Kemsley, O. B. Sutcliffe and R. E. Mewis, *ACS Omega*, 2019, **4**, 7103–7112.

42 S. Lodge, P. Nitschke, R. L. Loo, T. Kimhofer, S.-H. Bong, T. Richards, S. Begum, M. Spraul, H. Schaefer, J. C. Lindon, E. Holmes and J. K. Nicholson, *J. Proteome Res.*, 2021, **20**, 1415–1423.

43 Y. Su, D. Yuan, D. G. Chen, R. H. Ng, K. Wang, J. Choi, S. Li, S. Hong, R. Zhang, J. Xie, S. A. Kornilov, K. Scherler, A. J. Pavlovitch-Bedzyk, S. Dong, C. Lausted, I. Lee, S. Fallen, C. L. Dai, P. Baloni, B. Smith, V. R. Duvvuri, K. G. Anderson, J. Li, F. Yang, C. J. Duncombe, D. J. McCulloch, C. Rostomily, P. Troisch, J. Zhou, S. Mackay, Q. DeGottardi, D. H. May, R. Taniguchi, R. M. Gittelman, M. Klinger, T. M. Snyder, R. Roper, G. Wojciechowska, K. Murray, R. Edmark, S. Evans, L. Jones, Y. Zhou, L. Rowen, R. Liu, W. Chour, H. A. Algren, W. R. Berrington, J. A. Wallick, R. A. Cochran, M. E. Micikas, The ISB-Swedish COVID-19 Biobanking Unit, T. Wrin, C. J. Petropoulos, H. R. Cole, T. D. Fischer, W. Wei, D. S. B. Hoon, N. D. Price, N. Subramanian, J. A. Hill, J. Hadlock, A. T. Magis, A. Ribas, L. L. Lanier, S. D. Boyd, J. A. Bluestone, H. Chu, L. Hood, R. Gottardo, P. D. Greenberg, M. M. Davis, J. D. Goldman and J. R. Heath, *Cell*, 2022, **185**, 881–895.

44 X. Bi, W. Liu, X. Ding, S. Liang, Y. Zheng, X. Zhu, S. Quan, X. Yi, N. Xiang, J. Du, H. Lyu, D. Yu, C. Zhang, L. Xu, W. Ge, X. Zhan, J. He, Z. Xiong, S. Zhang, Y. Li, P. Xu, G. Zhu, D. Wang, H. Zhu, S. Chen, J. Li, H. Zhao, Y. Zhu, H. Liu, J. Xu, B. Shen and T. Guo, *Cell Rep.*, 2021, 110271.

45 S. Zhang, P. Luo, J. Xu, L. Yang, P. Ma, X. Tan, Q. Chen, M. Zhou, S. Song, H. Xia, S. Wang, Y. Ma, F. Yang, Y. Liu, Y. Li, G. Ma, Z. Wang, Y. Duan and Y. Jin, *J. Inflammation Res.*, 2021, **14**, 4485–4501.

46 J. D. Bell, J. C. C. Brown, J. K. Nicholson and P. J. Sadler, *FEBS Lett.*, 1987, **215**, 311–315.

47 J. A. Levine, J. M. Han, A. Wolska, S. R. Wilson, T. P. Patel, A. T. Remaley, V. Periwal, J. A. Yanovski and A. P. Demidowich, *J. Clin. Lipidol.*, 2020, **14**, 667–674.

48 A. O. Akinkuolie, A. D. Pradhan, J. E. Buring, P. M. Ridker and S. Mora, *Arterioscler. Thromb. Vasc. Biol.*, 2015, **35**, 1544–1550.

49 E. G. Gruppen, M. A. Connelly, W. J. Sluiter, S. J. L. Bakker and R. P. F. Dullaart, *Clin. Chim. Acta*, 2019, **488**, 7–12.

50 E. G. Gruppen, I. J. Riphagen, M. A. Connelly, J. D. Otvos, S. J. Bakker and R. P. Dullaart, *PLoS One*, 2015, **10**, e0139057.

51 J. Rodríguez-Carrio, M. Alperi-López, P. López, Á. I. Pérez-Álvarez, M. Gil-Serret, N. Amigó, C. Ulloa, L. Benavente, F. J. Ballina-García and A. Suárez, *J. Clin. Med. Res.*, 2020, **9**(8), 2472.

52 A.-I. Malo, A. Rull, J. Girona, P. Domingo, R. Fuertes-Martín, N. Amigó, C. Rodríguez-Borjabad, N. Martínez-Micaelo, M. Leal, J. Peraire, X. Correig, F. Vidal and L. Masana, *J. Clin. Med. Res.*, 2020, **9**(5), 1344.

53 R. P. Dullaart, E. G. Gruppen, M. A. Connelly, J. D. Otvos and J. D. Lefrandt, *Clin. Biochem.*, 2015, **48**, 811–814.

54 R. Masuda, S. Lodge, P. Nitschke, M. Spraul, H. Schaefer, S.-H. Bong, T. Kimhofer, D. Hall, R. L. Loo, M. Bizkarguenaga, C. Bruzzone, R. Gil-Redondo, N. Embade, J. M. Mato, E. Holmes, J. Wist, O. Millet and J. K. Nicholson, *J. Proteome Res.*, 2021, **20**, 4139–4152.

55 M. Liu, J. K. Nicholson and J. C. Lindon, *Anal. Chem.*, 1996, **68**, 3370–3376.

56 D. Baumstark, W. Kremer, A. Boettcher, C. Schreier, P. Sander, G. Schmitz, R. Kirchhoefer, F. Huber and H. R. Kalbitzer, *J. Lipid Res.*, 2019, **60**, 1516–1534.

57 J. D. Otvos, I. Shalaurova, J. Wolak-Dinsmore, M. A. Connelly, R. H. Mackey, J. H. Stein and R. P. Tracy, *Clin. Chem.*, 2015, **61**, 714–723.

58 J. K. Nicholson, M. P. O'Flynn, P. J. Sadler, A. F. Macleod, S. M. Juul and P. H. Sonksen, *Biochem. J.*, 1984, **217**, 365–375.

59 O. Beckonert, H. C. Keun, T. M. Ebbels, J. Bundy, E. Holmes, J. C. Lindon and J. K. Nicholson, *Nat. Protoc.*, 2007, **2**, 2692–2703.

60 T. Castaing-Cordier, D. Bouillaud, J. Farjon and P. Giraudeau, in *Annual Reports on NMR Spectroscopy*, ed. G. A. Webb, Academic Press, 2021, vol. 103, pp. 191–258.

61 M. Grootveld, B. Percival, M. Gibson, Y. Osman, M. Edgar, M. Molinari, M. L. Mather, F. Casanova and P. B. Wilson, *Anal. Chim. Acta*, 2019, **1067**, 11–30.

62 A. C. Dona, B. Jimenez, H. Schafer, E. Humpfer, M. Spraul, M. R. Lewis, J. T. Pearce, E. Holmes, J. C. Lindon and J. K. Nicholson, *Anal. Chem.*, 2014, **86**, 9887–9894.

63 E. K. Nawrocka, M. Urbańczyk, K. Koziński and K. Kazimierczuk, *RSC Adv.*, 2021, **11**, 35321–35325.

64 N. Bloembergen, E. M. Purcell and R. V. Pound, *Nature*, 1947, **160**, 475.

65 R. R. Ernst, G. Bodenhausen and A. Wokaun, *Principles of Nuclear Magnetic Resonance in One and Two Dimensions*, Clarendon Press, Oxford, 1987.